



Contents lists available at ScienceDirect

Atmospheric Environment

journal homepage: www.elsevier.com/locate/atmosenv

Effects of relative humidity on heterogeneous reaction of SO₂ with CaCO₃ particles and formation of CaSO₄·2H₂O crystal as secondary aerosol

Yang Yue^{a,b}, Jingru Cheng^a, Kang Soo Lee^a, Roman Stocker^a, Xu He^c, Maosheng Yao^d,
Jing Wang^{a,b,*}

^a Institute of Environmental Engineering, ETH Zurich, Zurich, 8093, Switzerland

^b Laboratory for Advanced Analytical Technologies, Empa, Swiss Federal Laboratories for Materials Science and Technology, Dübendorf, 8600, Switzerland

^c State Key Laboratory of Urban Water Resource and Environment, Harbin Institute of Technology, Harbin, 150090, China

^d State Key Joint Laboratory of Environmental Simulation and Pollution Control, College of Environmental Sciences and Engineering, Peking University, Beijing, 100871, China

HIGHLIGHTS

- Different types of CaSO₄·2H₂O crystals were observed in some urban ambient particulate matter samples.
- Lab controlled experiments indicated that relative humidity played a significant role in CaSO₄·2H₂O crystals formation.
- The study provides useful information to understand the secondary inorganic aerosol formation and air pollution control.

ARTICLE INFO

Keywords:

Haze event
Particulate matter
CaSO₄
Relative humidity
Sulfur dioxide
Secondary inorganic aerosol

ABSTRACT

Haze related air pollution has become one of major environmental concerns in some Asian countries. Sulfate is a main component of ambient particulate matter (PM) in the urban environment during haze episodes. Among the pollutants, sulfur dioxide (SO₂) is an important precursor of sulfate and new atmospheric particle formation. However, under different atmospheric conditions its underlying formation mechanisms are not clearly elucidated. In the current work, we collected ambient PM in two cities: Zurich (Switzerland) and Beijing (China). The PM morphology and the composition were investigated by scanning electron microscopy, energy dispersive X-Ray spectroscopy and Raman micro-spectroscopy. In addition, a series of lab controlled experiments were also performed to study the SO₂ reaction with CaCO₃ aerosol. We found different types of CaSO₄·2H₂O crystals in the Chinese urban samples, with clearly different compositions than those from Zurich. The experimental data showed that the relative humidity played a significant role on the new CaSO₄·2H₂O crystal formation including its size, morphology and composition. Relative humidity (RH) above 80% can significantly promote SO₂ oxidation on the CaCO₃ particles and form the CaSO₄·2H₂O crystals. In contrast, at relative humidity below 40%, only few CaCO₃ particles can be converted to CaSO₄ particles. The results of this study facilitate the understanding of secondary inorganic aerosol formation by the reaction of CaCO₃ particles with SO₂ with different RHs in different city environments, and provide useful information for air pollution control.

1. Introduction

In many Asian countries, including China and India, the main air pollution is the haze induced by ambient particulate matter (PM) (Boys et al., 2014; Huang et al., 2014; Jayarathne et al., 2016; Li et al., 2017, 2019). Ambient PM which contains mineral dust, metals, organic compounds and biological materials can lead to high risk for human

respiratory and cardiovascular systems. In the past years, the haze events occurred frequently and influenced large areas in China, India and other countries. These haze events also led to millions of premature deaths and inestimable economic losses (Balakrishnan et al., 2019; Liu et al., 2019a). Previous research showed that the severe haze pollution events in China were due to large emissions of primary air pollutants (e. g., SO₂, NO_x, NH₃, dust and smoke), local stagnant meteorological

* Corresponding author. Institute of Environmental Engineering, ETH Zurich, Zurich, 8093, Switzerland.
E-mail address: jing.wang@ifu.baug.ethz.ch (J. Wang).

<https://doi.org/10.1016/j.atmosenv.2021.118776>

Received 31 January 2021; Received in revised form 28 August 2021; Accepted 5 October 2021

Available online 11 October 2021

1352-2310/© 2021 The Authors. Published by Elsevier Ltd. This is an open access article under the CC BY license (<http://creativecommons.org/licenses/by/4.0/>).

conditions and fast formation of secondary aerosol, especially sulfate (SO_4^{2-}) and nitrate (NO_3^-) (Cheng et al., 2016; Guo et al., 2014; Huang et al., 2014). Sulfate is a major component of fine PM and the airborne concentration can be up to $300 \mu\text{g}/\text{m}^3$ during some haze events in Beijing (Cheng et al., 2016). Heterogeneous oxidation of SO_2 on solid or aqueous particles is thought to be a potentially important source of sulfate PM in the atmosphere (Takahashi et al., 2008; Yu et al., 2018; Zhao et al., 2018).

Primary ambient PM can be produced from different sources, such as construction, mining activity, landscaping maintenance activity, industrial emission, combustion and so on. Among the different components of PM, mineral dusts contribute a large fraction (30–60%) of global aerosols (Xu et al., 2011). Global mineral dust emissions are estimated at 1,000–5,000 million tons per year. Most of mineral dusts are oxides, e.g. CaO , FeO , Fe_2O_3 , SiO_2 , Al_2O_3 , as well as carbonates, e.g. CaCO_3 , MgCO_3 . These mineral dusts can be transported to urban areas by the winds such as dust storms. The primary air pollutants, e.g. SO_2 and NO_x , can react with ambient PM and form secondary inorganic aerosol to influence the ambient PM concentration, type, composition and toxicity (Longo et al., 2016; Yao et al., 2018). As China energy supply depends strongly on coal combustion, China has high surface concentration of SO_2 up to 100 ppb (Bauduin et al., 2016; Duan et al., 2006). With the effort of the Chinese government in air pollution control in the past years, the total emission of SO_2 has decreased in most parts of China. However, high concentrations of SO_2 are still frequently observed in some heavily polluted regions (Wang et al., 2015b, 2018). For instance, over 100 ppb SO_2 was measured in haze days during 2012 in Xi'an and the SO_2 concentration was up to 43 ppb in the winter of 2013 in Jinan (Wang et al., 2015a; Zhang et al., 2015). High concentrations of SO_2 may induce high concentrations of secondary inorganic component in $\text{PM}_{2.5}$ (particulate matter less than $2.5 \mu\text{m}$) during haze formation (Wang et al., 2012; Yang et al., 2011b; Yao et al., 2018; Zhao et al., 2013). SO_2 can be oxidized in the gas phase predominantly by OH, or in the particle phase by species such as O_3 (Wu et al., 2011), O_2 (Ma et al., 2013), or NO_2 (Li et al., 2010), and then form new sulfate PM. There are ample studies investigating the heterogeneous reactions of SO_2 on various particles, e.g. MgO (Goodman et al., 2001), ZnO (Li et al., 2011), mineral dust proxy particles (Huang et al., 2016), and CaCO_3 (Li et al., 2010; Zhao et al., 2018), etc. Researchers observed that the ambient calcite PM reacted with acidic SO_x species, e.g. SO_2 , sulfuric acid and acidic sulfate salts, and were transformed to gypsum during the transport from the west of China to Japan (Takahashi et al., 2006, 2009). This reaction neutralized acidic sulfur species and reduced the concentration of sulfate aerosol, one of the major components of cloud condensation nuclei (Miyamoto et al., 2020).

As a ubiquitous component in the atmosphere, water vapor has critical influence on the heterogeneous reaction of trace gases. Several studies suggested that the presence of water vapor can significantly promote the interaction of SO_2 and NO_2 with mineral particles, therefore inducing secondary inorganic aerosol formation (Mori et al., 1998; Tan et al., 2016; Zhang et al., 2018). For example, Li et al. (2006) found that water vapor absorption can enhance the capability of sulfate formation on the surface of CaCO_3 particles. Combined with water vapor, CaSO_4 can form $\text{CaSO}_4 \cdot 2\text{H}_2\text{O}$ molecules on CaCO_3 particles surface, providing new reaction active sites and promoting the reaction of SO_2 with CaCO_3 particles (Li et al., 2006). In addition, water vapor also increased the nitrate concentration on CaCO_3 particle surface by enhancing the absorption coefficient of NO_2 (Al-Hosney and Grassian, 2005; Li et al., 2010). Therefore, it is important to investigate the effect of ambient air oxidation and water vapor on the process of heterogeneous reaction of SO_2 on particles and the size of new sulfate PM in different environment scenarios.

In this work, the main goal was to study the differences of ambient PM morphology and composition between Beijing and Zurich in summer. Ambient PM samples were collected from both Beijing (China) and Zurich (Switzerland), two cities with a similar latitude. Beijing is in the

warm and temperate zone with hot and rainy summers, a typical continental monsoon climate (Yang et al., 2011a). In comparison, Zurich has a typical humid continental climate with lower temperature and shorter precipitation in summer. Based on the ambient sample analysis, a series of lab controlled simulation experiments were also performed to study the effects of ambient air oxidation, SO_2 and relative humidity on PM formation.

2. Material and methods

2.1. Sample collection

Current work aim to study the differences of PM composition and morphology from various locations with different levels of air pollution. To this end, we chose two cities, Beijing (China) and Zurich (Switzerland). Three sampling locations are shown in Fig. S1 (Supporting Information). The sampling site of Swiss Federal Laboratories for Materials Science and Technology (Empa) was close to the NABEL (National Air Pollution Monitoring Network) station at Empa, Zürich, which is a representative of a Swiss suburban campus. In China, two sampling sites in Beijing, Peking University campus and Zhongguancun North Str. close to Beijing 4th Ring were selected to represent the Beijing urban campus and urban main street, respectively. They were named as CH-suburban campus (samples from Empa, Switzerland), CN-urban campus (samples from Peking University, China) and CN-urban main street (samples from Zhongguancun North Str., China) to be effectively identified. During all sampling periods, no rainfall or strong wind were involved. All the samples were stored at -20°C until further analysis. The meteorological data, from Swiss NABEL and Beijing Municipal Environmental Monitoring Center for each sampling site during the sampling periods, were recorded for further analysis (Table 1).

2.2. PM analysis

The morphologies of the ambient PM samples were characterized by scanning electron microscopy (SEM, Phenom ProX, Eindhoven, Netherlands). PM samples on aluminium foils were mounted on aluminium stubs and were analyzed in secondary electron detector (SED) mode at 10 kV or 15 kV. All images were acquired at $5,000 \times$ or $10,000 \times$ magnification. The composition of ambient PM and simulated CaCO_3 , $\text{CaCO}_3/\text{CaSO}_4 \cdot 2\text{H}_2\text{O}$, $\text{CaSO}_4 \cdot 2\text{H}_2\text{O}$ particles were analyzed by energy dispersive X-ray analyser using the same SEM as above.

A confocal Raman microspectroscopy (LabRAM HR Evolution, Horiba Scientific, France) based on a commercial upright microscope (BX-41, Olympus) was also used to further investigate the composition of ambient PM and the reaction process of CaCO_3 to $\text{CaSO}_4 \cdot 2\text{H}_2\text{O}$. A continuous wave neodymium-doped yttrium aluminum garnet (Nd:YAG) 532-nm laser (Cobolt, Germany) was focused on PM sample (mounted on aluminium foil and then glass slide to fit on the microscope stage) using $100 \times$ dry objective (Olympus, Japan). 300 mW at the laser outlet with a subsequent 5% density filter resulted in 15 mW on the sample. 300-lines/mm grating, 100- μm pinhole size, and 10-s exposure time were used for the measurements.

For each relative humidity condition, 20–30 particles were measured and the data were processed using a software built in-house – smoothing using Savitzky-Golay filter (we used the polynomial order of 3 and the window size of 5, which led to the mild smoothing effect) (Orfanidis, 1995), followed by the polynomial-based baseline subtraction (we used the polynomial order of 3) (Mazet et al., 2005). To evaluate the conversion from CaCO_3 to $\text{CaSO}_4 \cdot 2\text{H}_2\text{O}$, we calculated $I_{930-1,040}/(I_{930-1,040} + I_{1,050-1,100})$, where $I_{930-1,040}$ and $I_{1,050-1,100}$ denote the integrated intensity of SO_4^{2-} and CO_3^{2-} peaks, respectively. The hydration status was detected using the spectral region 3,300–3,500 cm^{-1} .

Table 1
Meteorological data of sampling sites.

Sampling site	Time	Ave. T. (°C)	RH (%)	PM2.5 (µg/m ³)	PM10 (µg/m ³)	SO ₂ (µg/m ³)	Ozone (µg/m ³)
CH-suburban campus	13.06–14.06.2017	19.6–22.1	46%–92%	13.6–16.7	15.8–22.1	0.5–1.2	67–106
CN-urban campus	31.08–04.09.2017	22.9–24.1	50%–86%	102.3–118.1	137.0–151.2	2–7	90–174
CN-urban main street	07.09–08.09.2017	25.1–26.9	50%–85%	30.9–124.0	62.7–179.8	3–7	90–288

CH-suburban campus: Empa, Dübendorf, Switzerland; CN-urban campus: PKU campus, Beijing, China; CN-urban main street: Zhongguancun North Str., Beijing, China. Data source: Weather China, <http://www.weather.com.cn/>.

2.3. Lab controlled experiments

To investigate the formation of CaSO₄ aerosol and CaSO₄·2H₂O crystal, two different lab simulation experiments were performed in reaction chambers to simulate the static and aerosol states, respectively. In the first simulation, a 5 L reaction chamber was used to study the effect of relative humidity on CaSO₄·2H₂O crystal formation (Fig. 1A). CaCO₃ water suspension was applied on the surface of aluminium foils and put into the reaction chamber. The CaCO₃ suspension on aluminium foils was dried before performing experiments in order to study the effect of relative humidity (RH) in reaction chamber. In order to maintain the RH to a pre-defined range in the reaction chamber, the flow rate of compressed air, which brought moisture from the water bubbler to the reaction chamber, was adjusted to keep the RH in the reaction chamber as 40% ± 5%, 60% ± 5%, 80% ± 5% and 95%–100% (referred to as 100% in the following text). A RH sensor (SHTW2, Sensirion AG,

Switzerland) was also used to measure the RH in the chamber to confirm the stable RH condition. The SO₂ concentration was maintained in the range of 1–2 mg/L (385–770 ppm) in the reaction chamber. The gas at the outlet of the reaction chamber was collected in 1 M NaOH solution to remove the residual SO₂ before emitted to air. Each experiment lasted for 16 h. After reaction, the aluminium foils were cut to small pieces and mounted on SEM stubs for SEM and EDX analysis or on glass slides for Raman measurements.

In the second simulation, a homemade 200 L aerosol reaction chamber was employed to mimic the reaction of SO₂ with CaCO₃ in aerosol phase (Fig. 1B). The CaCO₃ aerosol was generated by an atomizer. The mass concentration of CaCO₃ suspension was 2% in nanopure water. The RH for the simulation was maintained as 40% ± 5%, 60% ± 5%, 75% ± 5%, 80% ± 5% and 100%. The SO₂ concentration was measured by a portable gas analyser (PEG-350E, HORIBA). By adjusting the mass flow controller, the SO₂ concentration was kept in the range of 100–200 ppm. The gas at the outlet of the reaction chamber was also collected in 1 M NaOH solution. After 6 h reaction, the aerosol was collected on aluminium foils and analyzed by SEM, EDX and Raman micro-spectroscopy.

2.4. Data analysis

All data were analyzed by GraphPad Prism version 6.01 for Windows (GraphPad Software Inc., San Diego, CA, USA). Graphs were prepared with GraphPad Prism. The ratio of sulfate in the total carbonate and sulfate Raman spectra were analyzed by one-way ANOVA and Tukey's multiple comparisons test. Values with *p*-value < 0.01 were considered to be statistically significant.

3. Results and discussion

3.1. CaSO₄ crystal in ambient samples

The morphology and composition of ambient PM from Beijing were significantly different from the PM samples from Zurich as shown in Fig. 2. Zurich PM samples tended to be more homogeneous in morphology and were mainly composed of carbon, oxygen, nitrogen, silicon, iron, etc. In contrast, different kinds of rod crystal particles were found in the Chinese PM samples. EDX results indicate that the main components of these crystal particles were carbon, sulfur, and oxygen. Raman spectra analysis showed a typical peak at 1,006 cm⁻¹, which is the symmetric stretching mode of gypsum (Ma et al., 2013). The results suggest that the rod crystal particles were mainly CaSO₄·2H₂O. Besides, in some crystal particles, another peak was detected at 1,050 cm⁻¹, which is assigned to the symmetric stretching mode of nitrate (Ilanoul et al., 2002; Sarma et al., 1998). These sulfate and nitrate signals indicate that some of crystal particles were heterogeneous. Furthermore, in the EDX analysis, both sulfur and nitrogen signals were also detected in those particles. Previous work reported that SO₂ could be oxidized to sulfate by O₂ (Martin and Good, 1991; Siefert et al., 1996), NO₂ (Cheng et al., 2016; Wang et al., 2016) and O₃ (Li et al., 2006; Wu et al., 2011). NO₂ could act as the initiator of radical formation during the SO₂ oxidation process by O₂, but not as the main oxidant (Yu et al., 2018). In the urban environment, e.g. Beijing, NO₂ concentration was also at a high level and it was possible to form these heterogeneous particles with

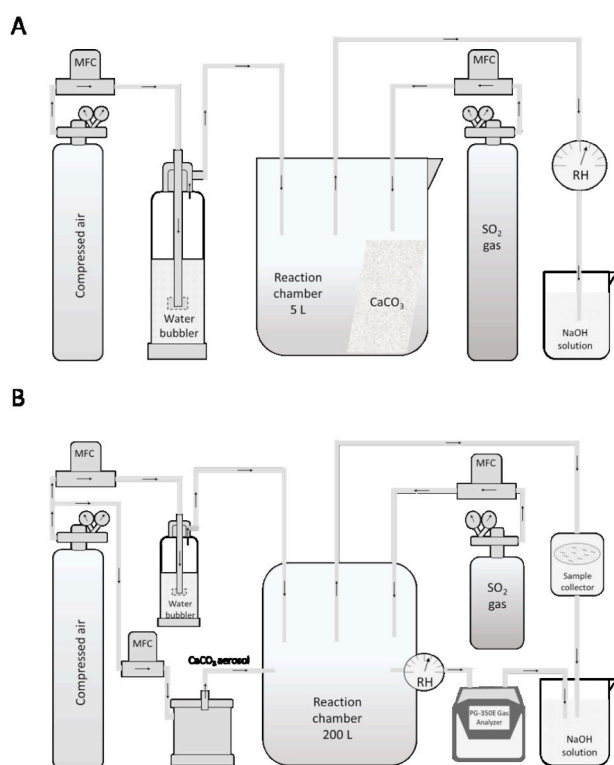


Fig. 1. The scheme of lab simulation chambers. A: the 5 L simulation chamber. CaCO₃ suspension was applied on aluminium foils surface. The relative humidity in the reaction chamber was maintained at 40% ± 5%, 60% ± 5%, 80% ± 5% and 95%–100% by a water bubbler. The SO₂ concentration was maintained in the range of 1–2 mg/L in the reaction chamber. Each experiment lasted for 16 h. B: the 200 L aerosol reaction chamber. MFC: mass flow controller. The CaCO₃ aerosol was generated by an atomizer. The SO₂ concentration was kept in the range of 100–200 ppm. Each experiment lasted for 6 h. All samples were analyzed by SEM, EDX and Raman micro-spectroscopy. In both experiments, the exhaust gas at the outlet of the reaction chamber was collected in 1 M NaOH solution to remove the residual SO₂ before emitted to air.

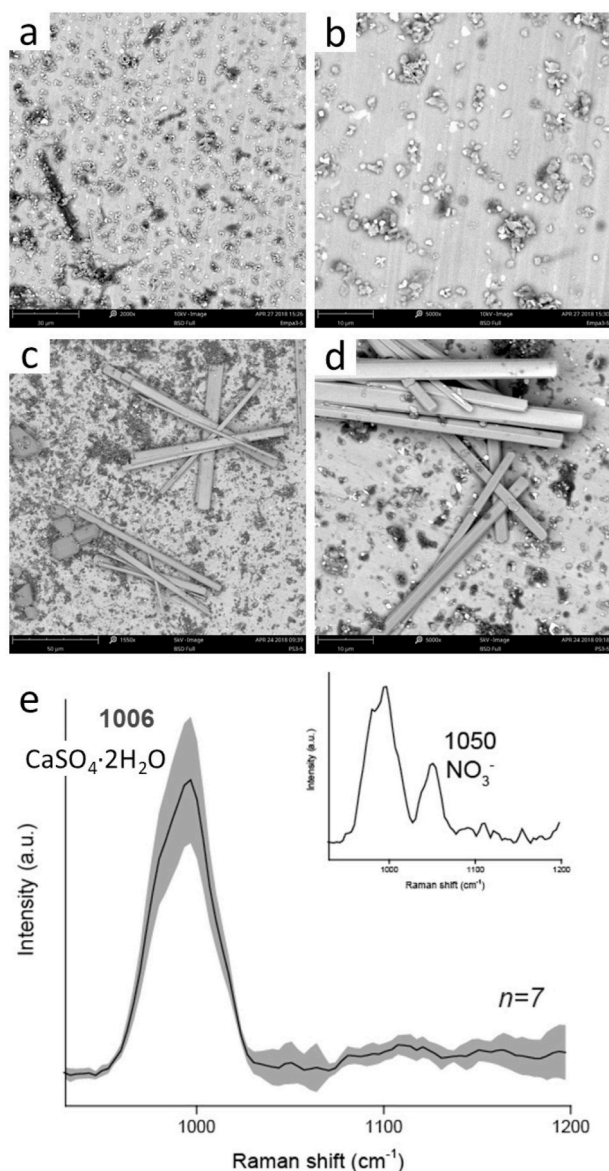


Fig. 2. The morphology and composition of ambient PM from Switzerland (a–b: CH-suburban) and China (c–d: CN-urban). The Raman spectra analysis of PM from China was shown in the panel e. The grey area in panel e indicated the measurement standard deviation.

both sulfate and nitrate. In the urban environment, e.g. Beijing ambient, NO_2 concentration was also at a high level and it was possible to form these heterogeneous particles with both sulfate and nitrate components, as demonstrated by our results.

Fig. 3 shows the elemental analysis of ambient PM collected from Zurich suburban and Beijing urban campuses. The PM collected from Zurich suburban environment showed major elements O, N, C, Si and Na (Fig. 3a–c). EDX analysis indicated that some of the amorphous particles (Fig. 3d–f) from Beijing urban environment contained O, Ca, C, S, N and Mg, which suggested that these particles were a mixture of carbonate, sulfate and nitrate. The crystalline particles collected from Beijing urban campus had diameters of 2–5 μm and lengths of 10–15 μm (Fig. 3g–i). Meanwhile, in the samples collected from Beijing urban main street, the crystalline particles were shorter and the lengths were only about 5–10 μm (Fig. 3j–l).

The formation of sulfate crystal has been reported in several studies. Shi et al. (2003) analyzed a variety of particles collected in Beijing in 2001 using SEM and EDX analyses which included mineral dust, coal fly

ash, soot aggregates as well as sulfates. Some sulfate particles were crystalline and contained S, Ca, K and Al, indicating that two or more phases of sulfates were present (Shi et al., 2003). Another work also collected ambient PM in the summer of Beijing and observed similar sulfate and nitrate crystalline particles (Liu et al., 2005) as the ones described in the present work.

3.2. Lab controlled experiments

Based on the elemental analysis results and previous studies, the calcium sulfate crystalline particles were assumed as secondary inorganic aerosol formed from the reaction of SO_2 with calcium carbonate. To verify this hypothesis, a two-step lab simulation experiment was performed. In the first step, the formation of $\text{CaSO}_4 \cdot 2\text{H}_2\text{O}$ from the reaction of SO_2 with calcium carbonate in suspension was tested in a 5 L reaction chamber under different levels of relative humidity. The CaCO_3 suspension on aluminum foils was dried before performing experiments in order to minimize the effect to RH in reaction chamber. In the second step, a 200 L reaction chamber was used to investigate the formation of $\text{CaSO}_4 \cdot 2\text{H}_2\text{O}$ crystal from the reaction of SO_2 with aerosol phase of calcium carbonate.

In the 5 L reaction system, significant formation of $\text{CaSO}_4 \cdot 2\text{H}_2\text{O}$ crystals was observed when the relative humidity was above 80%. As shown in Fig. 4, with the increase of relative humidity, more $\text{CaSO}_4 \cdot 2\text{H}_2\text{O}$ crystals with larger size were detected in the same field of view. In the 40% RH environment, only very low sulfur signal was detected in the EDX analysis. The SEM results indicated that most of CaCO_3 was still in amorphous state. When the RH increased to 60%, several small crystal clusters were observed among the amorphous CaCO_3 . In the simulation experiments with 80% of RH, more and larger $\text{CaSO}_4 \cdot 2\text{H}_2\text{O}$ crystals were detected. The morphology of $\text{CaSO}_4 \cdot 2\text{H}_2\text{O}$ crystals were almost the same as the crystalline particles in the Chinese urban campus ambient PM samples (CN-urban in Fig. 2). Under the condition of 100% RH, nearly all CaCO_3 reacted with SO_2 and formed even larger $\text{CaSO}_4 \cdot 2\text{H}_2\text{O}$ crystals.

Composition analysis by EDX and Raman microspectroscopy also revealed the heterogeneous reaction of SO_2 with CaCO_3 particles and the transformation of carbonate to sulfate (Fig. 5). The main fraction of particles were still kept in CaCO_3 and only 10%–40% of carbonate was transformed to sulfate in 40% RH after 16 h reaction. When the RH increased to 60%, 60%–90% of carbonate was converted to sulfate and formed small crystals. In the RH above 80%, almost all carbonate was transformed to sulfate and formed large $\text{CaSO}_4 \cdot 2\text{H}_2\text{O}$ crystals. EDX analysis indicated that the distribution of elemental percentage in these crystals was also close to that in those crystals collected in the China urban environment.

Formation of $\text{CaSO}_4 \cdot 2\text{H}_2\text{O}$ crystals from the reaction of SO_2 with aerosol phase CaCO_3 was tested in the 200 L reaction chamber. The SO_2 concentration was maintained at 100–200 ppm in the reaction chamber. Here, the relative humidity also strongly affected the formation of $\text{CaSO}_4 \cdot 2\text{H}_2\text{O}$ crystal. With the relative humidity of 45%–55%, the CaCO_3 aerosol did not react with SO_2 and no significant CaSO_4 was detected. When the relative humidity was increased to 80%–90%, a large amount of crystalline particles (Fig. 6) were collected in the size range of 0.5 μm –1.5 μm . Elemental analysis showed that the main components of these crystalline particles were O, S and Ca. The typical Raman spectra peak at 1,006 cm^{-1} and 1,136 cm^{-1} for gypsum (Ma et al., 2013) were also identified in the rod-like particles. Based on the element analysis results and Raman spectra results, the distribution of elemental percentage of these crystalline particles was similar to the $\text{CaSO}_4 \cdot 2\text{H}_2\text{O}$ crystals collected in the China urban environment and formed in lab simulation in the 5 L reaction chamber.

3.3. Potential mechanisms of sulfate formation

Previous research revealed that the formation of secondary inorganic

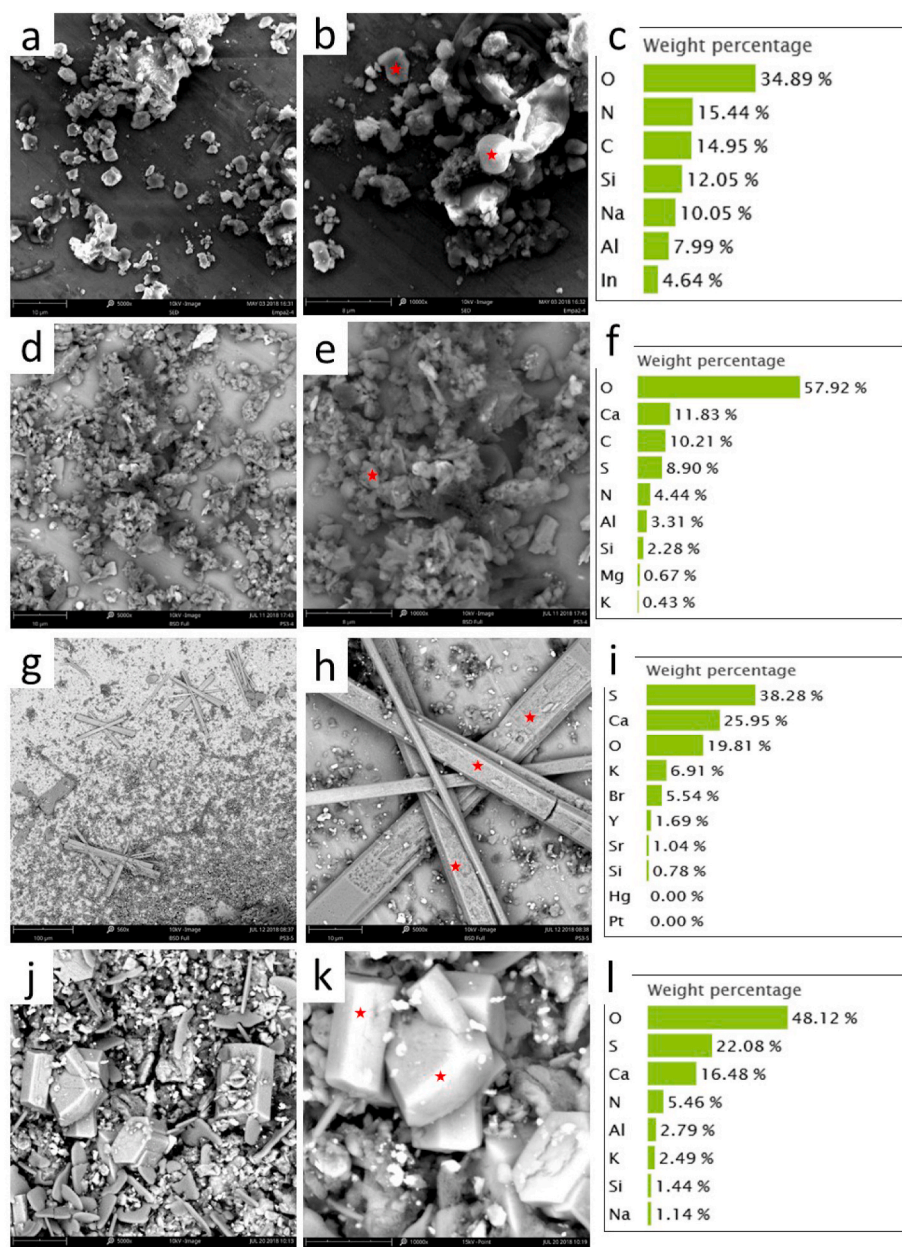


Fig. 3. The SEM images and EDX results of ambient PM from Zurich suburban (a–c) and Beijing urban (d–l) campuses. Panel a–c indicate particles from Zurich suburban campus. Panel d–f indicate amorphous particles from Beijing urban campus. Panel g–i indicate large rod crystal particles from Beijing urban campus. Panel j–l indicate small crystal particles from Beijing urban campus. The red asterisks indicate the EDX analysis sites. (For interpretation of the references to colour in this figure legend, the reader is referred to the Web version of this article.)

aerosol could happen in gaseous phase by reacting with hydroxyl radicals or in heterogeneous phase with seed aerosols, such as $\gamma\text{-Al}_2\text{O}_3$ (Huang et al., 2017; Lelieveld and Heintzenberg, 1992; Liu et al., 2012; Paulson et al., 1992). Oxidation of SO_2 on CaCO_3 has been studied in several conditions, a number of them with the coexisting NO_2 and ozone (Wang et al., 2016; Wu et al., 2011; Zhang et al., 2018).

Relative humidity and adsorbed water play an important role in the uptake and oxidation of atmospheric gases on carbonate aerosols. Studies on the SO_2 deposition on marble stone surface showed that the deposition velocity was around 5 times higher in humid air when condensed moisture formed on the stone surface than on dry samples (Cobourn et al., 1993). In a multiphase oxidation of SO_2 by NO_2 on CaCO_3 aerosols, it has been found that SO_2 oxidation was too slow to be detected at RH of 17%, whereas a significantly higher reactive uptake coefficient of SO_2 was observed for sulfate formation when RH was above 46% (Zhao et al., 2018). These results indicate that moisture can significantly enhance the uptake coefficient of ambient SO_2 on carbonate aerosols. In ambient air, CaCO_3 aerosol can adsorb water vapor and

form a thin water layer, which had a complex structure and showed phase transitions different from bulk liquid water. The adsorbed water molecules in the surface phase transition layers increased surface ionic mobility and enhanced the extent of reaction (Al-Hosney and Grassian, 2005; Baltrusaitis et al., 2007; Hausner et al., 2007).

Infrared spectroscopy has been used to study the interaction of H_2O , SO_2 and NO_2 with CaCO_3 particles and it was found that carbonic acid could adsorb on CaCO_3 surface. The adsorbed carbonic acid could form a $\text{Ca}(\text{OH})(\text{CO}_3\text{H})$ surface layer in the reaction of CaCO_3 and SO_2 when CaCO_3 particles were exposed to the ambient environment (Al-Hosney and Grassian, 2005). In the high relative humidity environment, water vapor could also adsorb on the CaCO_3 particles surface and promote dissociation of adsorbed carbonic acid, which increased the reactive uptake coefficient of SO_2 . The main products were calcium sulfite and calcium sulfate in the reaction of SO_2 with $\text{Ca}(\text{OH})(\text{CO}_3\text{H})$. Sulfite and sulfate microcrystallites were also observed in several lab simulation studies (Al-Hosney and Grassian, 2005; Stipp, 1999). At low relative humidity and low coverage, the water formed small islands and ordered

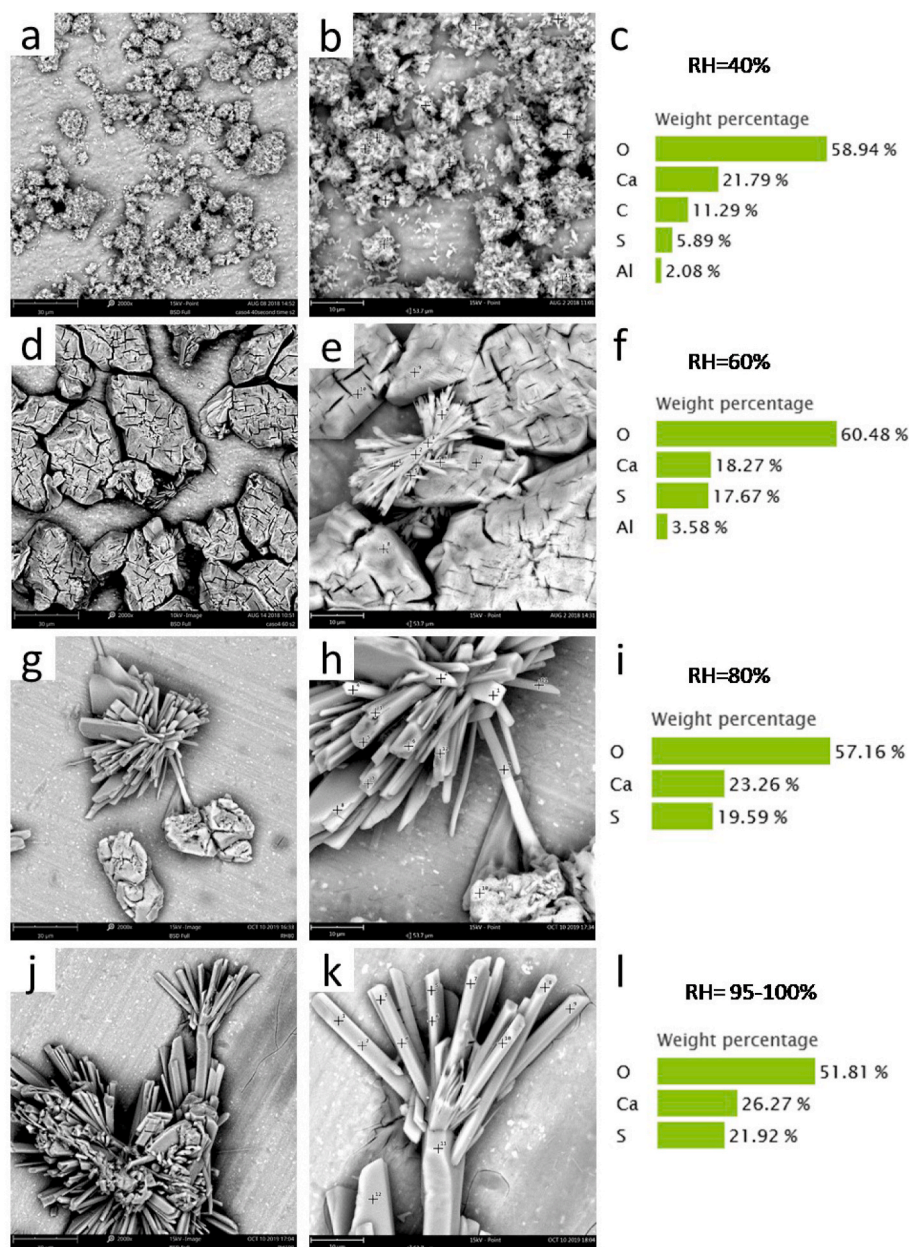


Fig. 4. The $\text{CaSO}_4 \cdot 2\text{H}_2\text{O}$ crystals generated by SO_2 and CaCO_3 suspension in the 5 L reaction chamber at different levels of relative humidity. Panel a–c: $\text{CaSO}_4 \cdot 2\text{H}_2\text{O}$ crystals generated under 40% of RH. Panel d–f: $\text{CaSO}_4 \cdot 2\text{H}_2\text{O}$ crystals generated under 60% of RH. Panel g–i: $\text{CaSO}_4 \cdot 2\text{H}_2\text{O}$ crystals generated under 80% of RH. Panel j–l: $\text{CaSO}_4 \cdot 2\text{H}_2\text{O}$ crystals generated under 95–100% of RH. The grey crosses indicate the EDX analysis sites.

ice-like structure on CaCO_3 surface and the phase was close to solid water. Whereas, at RH above 50%, the water molecules started to cluster together to form a disordered liquid-like water structure on CaCO_3 surface and the phase was close to liquid water (Al-Hosney and Grassian, 2005).

Therefore, at high relative humidity, water adsorption could enhance SO_2 uptake and reaction with $\text{Ca}(\text{OH})(\text{CO}_3\text{H})$ on the CaCO_3 surface. It was found that generated sulfite and sulfate could adsorb water and form 3D calcium sulfite hydrate structure, which trapped more water on the particle surface. The high ion mobility in the liquid-like water structure provided suitable environment for calcium sulfite and sulfate to form microcrystallites. The formed microcrystallites extended the reactive surface and sites to the CaCO_3 surface underneath and promoted whole CaCO_3 particles to transfer to sulfate finally (Cobourn et al., 1993; Fenter et al., 1995).

Heterogeneous oxidation of SO_2 on surfaces of aerosol particles is

considered to be an important pathway of sulfate formation in the atmosphere during haze events. The sulfate crystal particles were also observed during lab stimulation (Yu et al., 2018; Zhao et al., 2011), but few reports were available on the large size sulfate crystal particles in environmental samples. The current work observed huge amount of large size sulfate crystal particles and confirmed the formation of sulfate crystal particles in special environmental scenario, e.g. high relative humidity, SO_2 concentration and long reaction time, based on a series of lab simulation work. The results suggested that the different morphologies of sulfate may be due to two reasons: primary emission and environment factors. According to previous sources apportionment researches (Gao et al., 2018; Rai et al., 2021), the local sources of $\text{PM}_{2.5}$ in Beijing were coal, traffic, industry, construction dust and biomass. The secondary aerosol contributed 25%–50% to the local $\text{PM}_{2.5}$ in Beijing (Liu et al., 2019b). During the current project period, the ambient SO_2 and ozone in Beijing was 2–7 $\mu\text{g}/\text{m}^3$ and 90–288 $\mu\text{g}/\text{m}^3$ (Table 1),

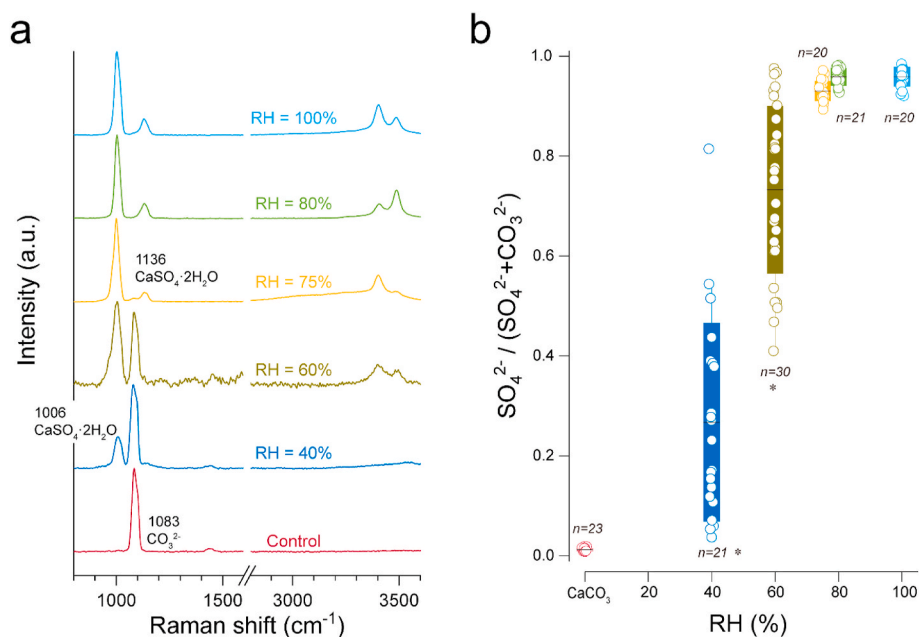


Fig. 5. Raman spectra of CaCO_3 particles during the reaction with SO_2 (100–200 ppm) at 40%, 60%, 75%, 80% and 100% RH. Panel a: the representative Raman spectra of individual $\text{CaCO}_3/\text{CaSO}_4 \cdot 2\text{H}_2\text{O}$ particles. The peak at 3300–3500 cm^{-1} indicates the hydration in crystal particles (Brotton and Kaiser, 2013). Panel b: the ratio of sulfate in the total carbonate and sulfate; 20–30 (n) samples were analyzed for each condition. The top and bottom edges of the box represent the 25th and 75th percentiles and the whisker represent the min to max values. Asterisks indicates that the ratio of sulfate at 40% and 60% RH are significantly lower than 75%, 80% and 100% RH, $p < 0.01$.

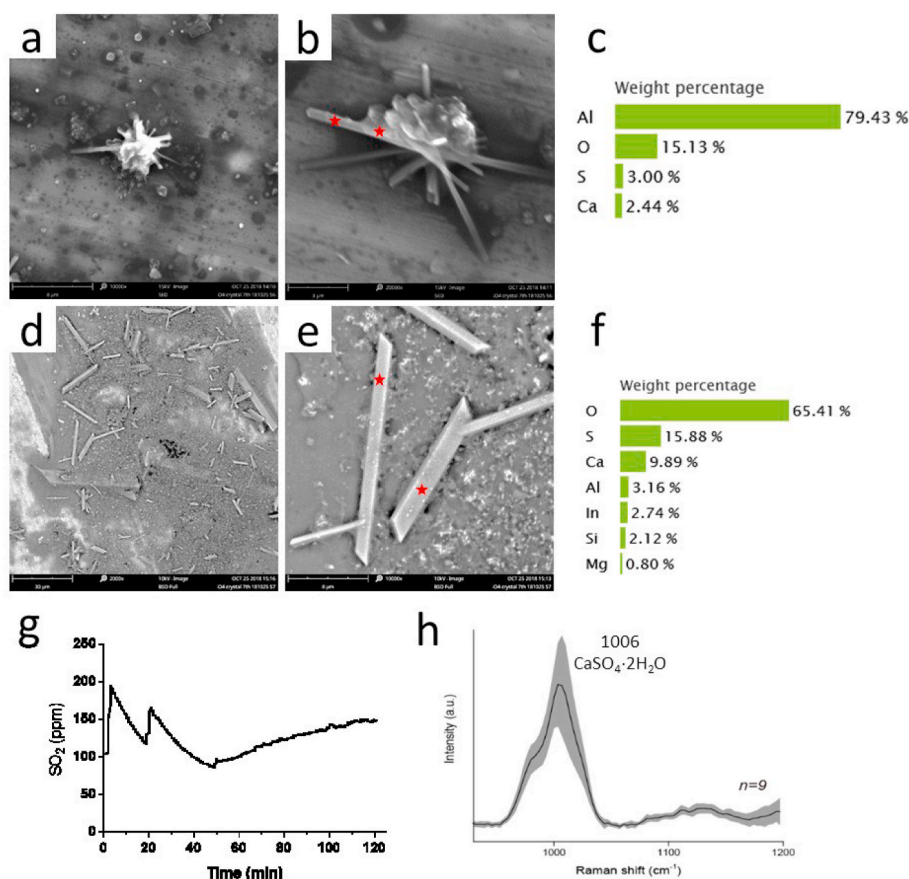


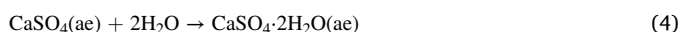
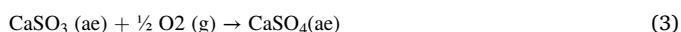
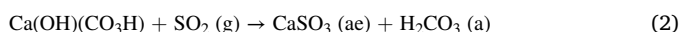
Fig. 6. The $\text{CaSO}_4 \cdot 2\text{H}_2\text{O}$ crystal generated by SO_2 and CaCO_3 aerosol in 200 L aerosol reaction chamber. Panel a–f: two different type of $\text{CaSO}_4 \cdot 2\text{H}_2\text{O}$ crystals and EDX analysis. Panel g: SO_2 concentration during lab simulation. Panel h: Raman spectra analysis of samples in panel d–e. The red asterisks indicate the EDX analysis sites. (For interpretation of the references to colour in this figure legend, the reader is referred to the Web version of this article.)

respectively. While in Zurich, the main primary emission source of PM10 was traffic and mineral dust, and the secondary aerosol contribution in Zurich was more than 50% in summer (Gianini et al., 2013). The ambient SO_2 and ozone in Zurich during the current project period

was only 0.5–1.2 $\mu\text{g}/\text{m}^3$ and 67–106 $\mu\text{g}/\text{m}^3$, respectively. Even though the ambient SO_2 concentration in Beijing was much lower than the air quality reference concentration, the SO_2 was still 3–4.9 times higher than Zurich. The ambient ozone in Beijing was 2.8 times of WHO

reference and much higher than Zurich. In Beijing, the high concentration of ozone may increase the heterogeneous oxidation of SO₂ with dust particles, which was another important primary emission in Beijing PM, and produced sulfate. The water vapor in high relative humidity may promote this oxidation process and induce the formation of large size sulfate crystal particles.

Here, we assimilate the previous mechanism studies and summarize formation of crystalline CaSO₄·2H₂O particles in two steps. Firstly, on reactive sites of CaCO₃ surface, such as oxygen atoms, hydroxyl groups or metal atoms, SO₂ reacts with water vapor and forms sulfite (Goodman et al., 2001). Then, sulfite products are oxidized to sulfate in the presence of oxidants, e.g. O₂, (Ma et al., 2013).



ae: aerosol phase; g: gas phase; s: solid phase; a: aqueous phase.

4. Conclusions

In the present work, we found several types of sulfate aerosols, especially calcium sulfate crystal, in the ambient PM samples from Beijing. In contrast, only amorphous sulfate was observed in the ambient PM samples in Zurich. We found that relative humidity had strong influence on the crystalline CaSO₄·2H₂O particles formation during the reaction of SO₂ with calcium carbonate. Relative humidity above 80% can significantly promote SO₂ oxidation on the CaCO₃ particles and formation of the CaSO₄·2H₂O crystals. In contrast, at relative humidity below 40%, only few CaCO₃ particles can be converted to CaSO₄ particles.

There are significantly higher levels of SO₂ and NO₂ during some haze episodes (Wang et al., 2016; Zhang et al., 2014). Oxidation by O₂ was considered an important source of sulfate and a sink of SO₂, which could affect the ambient SO₂ concentration and lifetime (Yu et al., 2018). The lifetime of SO₂ in the presence of NO₂ at 72% RH was around 20 days (Yu et al., 2018). The newly formed sulfate particles and crystals could further accelerate the multiphase oxidation of SO₂ by O₂ by providing the reactive surface and aerosol water content. In this way, this multiphase oxidation process could contribute significantly to the haze events which happened frequently in Chinese cities and other countries with heavy air pollution. It could also affect the ambient SO₂ concentration, sulfate PM concentration and morphology. Moreover, in the current work, the secondary sulfate PM was mainly small amorphous particles in low RH environment and large crystals in high RH environment. Recent work suggested that sulfate was a major constituent of fine PM in the haze events, especially in the winter season (Cheng et al., 2016). The results of this study facilitate the understanding of secondary inorganic aerosol formation by the reaction of CaCO₃ particles with SO₂, and provide useful information for the secondary inorganic aerosol research and the air quality control.

Data availability

The data used in this study are available from the corresponding author upon request (Prof. Jing Wang, jing.wang@ifu.baug.ethz.ch).

Author contributions

YY and JW designed this research. YY, MY and JW planned this campaign. YY and JC performed the lab controlled experiments. YY, JC and KL conducted samples analysis. YY analyzed data and wrote the manuscript. YY, KL, MY and JW contributed to the revisions of this

manuscript. All other co-authors participated in results discussion and manuscript editing.

Declaration of competing interest

The authors declare that they have no known competing financial interests or personal relationships that could have appeared to influence the work reported in this paper.

Acknowledgements

The study was partially supported by the Clean Air China Programme sponsored by Swiss Agency for Development and Cooperation, Switzerland. We thank Dr. Joachim Mohn (Empa, Swiss Federal Laboratories for Materials Science and Technology, Dübendorf, Switzerland) for SO₂ measurement.

Appendix A. Supplementary data

Supplementary data to this article can be found online at <https://doi.org/10.1016/j.atmosenv.2021.118776>.

References

- Al-Hosney, H.A., Grassian, V.H., 2005. Water, sulfur dioxide and nitric acid adsorption on calcium carbonate: a transmission and ATR-FTIR study. *Phys. Chem. Chem. Phys.* 7, 1266–1276.
- Balakrishnan, K., Dey, S., Gupta, T., Dhaliwal, R.S., Brauer, M., Cohen, A.J., Stanaway, J. D., Beig, G., Joshi, T.K., Aggarwal, A.N., Sabde, Y., Sadhu, H., Frostad, J., Causey, K., Godwin, W., Shukla, D.K., Kumar, G.A., Varghese, C.M., Muraleedharan, P., Agrawal, A., Anjana, R.M., Bhansali, A., Bhardwaj, D., Burkart, K., Cercy, K., Chakma, J.K., Chowdhury, S., Christopher, D.J., Dutta, E., Furtado, M., Ghosh, S., Ghoshal, A.G., Glenn, S.D., Guleria, R., Gupta, R., Jeemon, P., Kant, R., Kant, S., Kaur, T., Koul, P.A., Krish, V., Krishna, B., Larson, S.L., Madhipatla, K., Mahesh, P.A., Mohan, V., Mukhopadhyay, S., Mutreja, P., Naik, N., Nair, S., Nguyen, G., Odell, C. M., Pandian, J.D., Prabhakaran, D., Prabhakaran, P., Roy, A., Salvi, S., Sambandam, S., Saraf, D., Sharma, M., Shrivastava, A., Singh, V., Tandon, N., Thomas, N.J., Torre, A., Xavier, D., Yadav, G., Singh, S., Shekhar, C., Vos, T., Dandona, R., Reddy, K.S., Lim, S.S., Murray, C.J.L., Venkatesh, S., Dandona, L., 2019. The impact of air pollution on deaths, disease burden, and life expectancy across the states of India: the Global Burden of Disease Study 2017. *The Lancet Planet. Health* 3, e26–e39.
- Baltrusaitis, J., Usher, C.R., Grassian, V.H., 2007. Reactions of sulfur dioxide on calcium carbonate single crystal and particle surfaces at the adsorbed water carbonate interface. *Phys. Chem. Chem. Phys.* 9, 3011–3024.
- Bauduin, S., Clarisse, L., Hadji-Lazaro, J., Theys, N., Clerbaux, C., Coheur, P.F., 2016. Retrieval of near-surface sulfur dioxide (SO₂) concentrations at a global scale using IASI satellite observations. *Atmos. Meas. Tech.* 9, 721–740.
- Boys, B.L., Martin, R.V., van Donkelaar, A., MacDonell, R.J., Hsu, N.C., Cooper, M.J., Yantosca, R.M., Lu, Z., Streets, D.G., Zhang, Q., Wang, S.W., 2014. Fifteen-year global time series of satellite-derived fine particulate matter. *Environ. Sci. Technol.* 48, 11109–11118.
- Brotton, S.J., Kaiser, R.L., 2013. In situ Raman spectroscopic study of gypsum (CaSO₄·2H₂O) and epsomite (MgSO₄·7H₂O) dehydration utilizing an ultrasonic levitator. *J. Phys. Chem. Lett.* 4, 669–673.
- Cheng, Y., Zheng, G., Wei, C., Mu, Q., Zheng, B., Wang, Z., Gao, M., Zhang, Q., He, K., Carmichael, G., Pöschl, U., Su, H., 2016. Reactive nitrogen chemistry in aerosol water as a source of sulfate during haze events in China. *Sci. Adv.* 2, e1601530.
- Cobourn, W.G., Gauri, K.L., Tambe, S., Li, S., Saltik, E., 1993. Laboratory measurements of sulfur dioxide deposition velocity on marble and dolomite stone surfaces. *Atmospheric Environment. Part B. Urban Atmos.* 27, 193–201.
- Duan, F.K., He, K.B., Ma, Y.L., Yang, F.M., Yu, X.C., Cadle, S.H., Chan, T., Mulawa, P.A., 2006. Concentration and chemical characteristics of PM_{2.5} in Beijing, China: 2001–2002. *Sci. Total Environ.* 355, 264–275.
- Fenter, F.F., Caloz, F., Rossi, M.J., 1995. Experimental evidence for the efficient “dry deposition” of nitric acid on calcite. *Atmos. Environ.* 29, 3365–3372.
- Gao, J., Wang, K., Wang, Y., Liu, S., Zhu, C., Hao, J., Liu, H., Hua, S., Tian, H., 2018. Temporal-spatial characteristics and source apportionment of PM_{2.5} as well as its associated chemical species in the Beijing-Tianjin-Hebei region of China. *Environ. Pollut.* 233, 714–724.
- Gianini, M.F.D., Piot, C., Herich, H., Besombes, J.L., Jaffrezou, J.L., Hueglin, C., 2013. Source apportionment of PM₁₀, organic carbon and elemental carbon at Swiss sites: an intercomparison of different approaches. *Sci. Total Environ.* 454–455, 99–108.
- Goodman, A.L., Li, P., Usher, C.R., Grassian, V.H., 2001. Heterogeneous uptake of sulfur dioxide on aluminum and magnesium oxide particles. *J. Phys. Chem.* 105, 6109–6120.
- Guo, S., Hu, M., Zamora, M.L., Peng, J., Shang, D., Zheng, J., Du, Z., Wu, Z., Shao, M., Zeng, L., Molina, M.J., Zhang, R., 2014. Elucidating severe urban haze formation in China. *Proc. Natl. Acad. Sci. Unit. States Am.* 111, 17373–17378.

- Hausner, D.B., Reeder, R.J., Strongin, D.R., 2007. Humidity-induced restructuring of the calcite surface and the effect of divalent heavy metals. *J. Colloid Interface Sci.* 305, 101–110.
- Huang, L., Zhao, Y., Li, H., Chen, Z., 2016. Hydrogen peroxide maintains the heterogeneous reaction of sulfur dioxide on mineral dust proxy particles. *Atmos. Environ.* 141, 552–559.
- Huang, R.-J., Zhang, Y., Bozzetti, C., Ho, K.-F., Cao, J.-J., Han, Y., Daellenbach, K.R., Slowik, J.G., Platt, S.M., Canonaco, F., Zotter, P., Wolf, R., Pieber, S.M., Brunts, E.A., Crippa, M., Ciarelli, G., Piazzalunga, A., Schwikowski, M., Abbaszade, G., Schnelle-Kreis, J., Zimmermann, R., An, Z., Szidat, S., Baltensperger, U., Haddad, I.E., Prévôt, A.S.H., 2014. High secondary aerosol contribution to particulate pollution during haze events in China. *Nature* 514, 218.
- Huang, Z., Zhang, Z., Kong, W., Feng, S., Qiu, Y., Tang, S., Xia, C., Ma, L., Luo, M., Xu, D., 2017. Synergistic effect among Cl₂, SO₂ and NO₂ in their heterogeneous reactions on gamma-alumina. *Atmos. Environ.* 166, 403–411.
- Ianoul, A., Coleman, T., Asher, S.A., 2002. UV resonance Raman spectroscopic detection of nitrate and nitrite in wastewater treatment processes. *Anal. Chem.* 74, 1458–1461.
- Jayarathne, T., Rathnayake, C.M., Stone, E.A., 2016. Local source impacts on primary and secondary aerosols in the Midwestern United States. *Atmos. Environ.* 130, 74–83.
- Lelieveld, J., Heintzenberg, J., 1992. Sulfate cooling effect on climate through in-cloud oxidation of anthropogenic SO₂. *Science* 258, 117.
- Li, H.-J., Zhu, T., Zhao, D.F., Zhang, Z.F., Chen, Z.M., 2010. Kinetics and mechanisms of heterogeneous reaction of NO₂ on CaCO₃ surfaces under dry and wet conditions. *Atmos. Chem. Phys.* 10, 463–474.
- Li, J., Chen, H., Li, X., Wang, M., Zhang, X., Cao, J., Shen, F., Wu, Y., Xu, S., Fan, H., Da, G., Huang, R.-j., Wang, J., Chan, C.K., De Jesus, A.L., Morawska, L., Yao, M., 2019. Differing toxicity of ambient particulate matter (PM) in global cities. *Atmos. Environ.* 212, 305–315.
- Li, J., Shang, J., Zhu, T., 2011. Heterogeneous reactions of SO₂ on ZnO particle surfaces. *Sci. China Chem.* 54, 161–166.
- Li, L., Chen, Z.M., Zhang, Y.H., Zhu, T., Li, J.L., Ding, J., 2006. Kinetics and mechanism of heterogeneous oxidation of sulfur dioxide by ozone on surface of calcium carbonate. *Atmos. Chem. Phys.* 6, 2453–2464.
- Li, Y.J., Sun, Y., Zhang, Q., Li, X., Li, M., Zhou, Z., Chan, C.K., 2017. Real-time chemical characterization of atmospheric particulate matter in China: a review. *Atmos. Environ.* 158, 270–304.
- Liu, C., Chen, R., Sera, F., Vicedo-Cabrera, A.M., Guo, Y., Tong, S., Coelho, M.S.Z.S., Saldiva, P.H.N., Lavigne, E., Matus, P., Valdes Ortega, N., Osorio Garcia, S., Pascal, M., Stafoggia, M., Scortichini, M., Hashizume, M., Honda, Y., Hurtado-Díaz, M., Cruz, J., Nunes, B., Teixeira, J.P., Kim, H., Tobias, A., Íñiguez, C., Forsberg, B., Åström, C., Ragettli, M.S., Guo, Y.-L., Chen, B.-Y., Bell, M.L., Wright, C. Y., Scovronick, N., Garland, R.M., Milojevic, A., Kyselý, J., Urban, A., Orru, H., Indermitte, E., Jaakkola, J.J.K., Ryti, N.R.I., Katsouyanni, K., Analitis, A., Zanobetti, A., Schwartz, J., Chen, J., Wu, T., Cohen, A., Gasparrini, A., Kan, H., 2019a. Ambient particulate air pollution and daily mortality in 652 cities. *N. Engl. J. Med.* 381, 705–715.
- Liu, C., Ma, Q., Liu, Y., Ma, J., He, H., 2012. Synergistic reaction between SO₂ and NO₂ on mineral oxides: a potential formation pathway of sulfate aerosol. *Phys. Chem. Chem. Phys.* 14, 1668–1676.
- Liu, X., Zhu, J., Van Espen, P., Adams, F., Xiao, R., Dong, S., Li, Y., 2005. Single particle characterization of spring and summer aerosols in Beijing: formation of composite sulfate of calcium and potassium. *Atmos. Environ.* 39, 6909–6918.
- Liu, Y., Zheng, M., Yu, M., Cai, X., Du, H., Li, J., Zhou, T., Yan, C., Wang, X., Shi, Z., Harrison, R.M., Zhang, Q., He, K., 2019b. High-time-resolution source apportionment of PM_{2.5} in Beijing with multiple models. *Atmos. Chem. Phys.* 19, 6595–6609.
- Longo, A.F., Vine, D.J., King, L.E., Oakes, M., Weber, R.J., Huey, L.G., Russell, A.G., Ingall, E.D., 2016. Composition and oxidation state of sulfur in atmospheric particulate matter. *Atmos. Chem. Phys.* 16, 13389–13398.
- Ma, Q., He, H., Liu, Y., Liu, C., Grassian, V.H., 2013. Heterogeneous and multiphase formation pathways of gypsum in the atmosphere. *Phys. Chem. Chem. Phys.* 15, 19196–19204.
- Martin, L.R., Good, T.W., 1991. Catalyzed oxidation of sulfur dioxide in solution: the iron-manganese synergism. *Atmos. Environ. Part A. General Topics* 25, 2395–2399.
- Mazet, V., Carteret, C., Brie, D., Idier, J., Humbert, B., 2005. Background removal from spectra by designing and minimising a non-quadratic cost function. *Chemometr. Intell. Lab. Syst.* 76, 121–133.
- Miyamoto, C., Sakata, K., Yamakawa, Y., Takahashi, Y., 2020. Determination of calcium and sulfate species in aerosols associated with the conversion of its species through reaction processes in the atmosphere and its influence on cloud condensation nuclei activation. *Atmos. Environ.* 223, 117193.
- Mori, I., Nishikawa, M., Iwasaka, Y., 1998. Chemical reaction during the coagulation of ammonium sulphate and mineral particles in the atmosphere. *Sci. Total Environ.* 224, 87–91.
- Orfanidis, S.J., 1995. Introduction to signal processing. Prentice-Hall, Inc.
- Paulson, S.E., Flagan, R.C., Seinfeld, J.H., 1992. Atmospheric photooxidation of isoprene part I: the hydroxyl radical and ground state atomic oxygen reactions. *Int. J. Chem. Kinet.* 24, 79–101.
- Rai, P., Furger, M., Slowik, J.G., Zhong, H., Tong, Y., Wang, L., Duan, J., Gu, Y., Qi, L., Huang, R.-J., Cao, J., Baltensperger, U., Prévôt, A.S.H., 2021. Characteristics and sources of hourly elements in PM₁₀ and PM_{2.5} during wintertime in Beijing. *Environ. Pollut.* 278, 116865.
- Sarma, L.P., Prasad, P.S.R., Ravikumar, N., 1998. Raman spectroscopic study of phase transitions in natural gypsum. *J. Raman Spectrosc.* 29, 851–856.
- Shi, Z., Shao, L., Jones, T.P., Whittaker, A.G., Lu, S., Bérubé, K.A., He, T., Richards, R.J., 2003. Characterization of airborne individual particles collected in an urban area, a satellite city and a clean air area in Beijing, 2001. *Atmos. Environ.* 37, 4097–4108.
- Siefert, R.L., Webb, S.M., Hoffmann, M.R., 1996. Determination of photochemically available iron in ambient aerosols. *J. Geophys. Res.: Atmospheres* 101, 14441–14449.
- Stipp, S.L.S., 1999. Toward a conceptual model of the calcite surface: hydration, hydrolysis, and surface potential. *Geochem. Cosmochim. Acta* 63, 3121–3131.
- Takahashi, Y., Kanai, Y., Kamioka, H., Ohta, A., Maruyama, H., Song, Z., Shimizu, H., 2006. Speciation of sulfate in size-fractionated aerosol particles using sulfur K-edge X-ray absorption near-edge structure. *Environ. Sci. Technol.* 40, 5052–5057.
- Takahashi, Y., Miyoshi, T., Higashi, M., Kamioka, H., Kanai, Y., 2009. Neutralization of calcite in mineral aerosols by acidic sulfur species collected in China and Japan studied by Ca K-edge X-ray absorption near-edge structure. *Environ. Sci. Technol.* 43, 6535–6540.
- Takahashi, Y., Miyoshi, T., Yabuki, S., Inada, Y., Shimizu, H., 2008. Observation of transformation of calcite to gypsum in mineral aerosols by Ca K-edge X-ray absorption near-edge structure (XANES). *Atmos. Environ.* 42, 6535–6541.
- Tan, F., Tong, S., Jing, B., Hou, S., Liu, Q., Li, K., Zhang, Y., Ge, M., 2016. Heterogeneous reactions of NO₂ with CaCO₃–(NH₄)₂SO₄ mixtures at different relative humidities. *Atmos. Chem. Phys.* 16, 8081–8093.
- Wang, G., Zhang, R., Gomez, M.E., Yang, L., Levy Zamora, M., Hu, M., Lin, Y., Peng, J., Guo, S., Meng, J., Li, J., Cheng, C., Hu, T., Ren, Y., Wang, Y., Gao, J., Cao, J., An, Z., Zhou, W., Li, G., Wang, J., Tian, P., Marrero-Ortiz, W., Secret, J., Du, Z., Zheng, J., Shang, D., Zeng, L., Shao, M., Wang, W., Huang, Y., Wang, Y., Zhu, Y., Li, Y., Hu, J., Pan, B., Cai, L., Cheng, Y., Ji, Y., Zhang, F., Rosenfeld, D., Liss, P.S., Duce, R.A., Kolb, C.E., Molina, M.J., 2016. Persistent sulfate formation from London Fog to Chinese haze. *Proc. Natl. Acad. Sci. Unit. States Am.* 113, 13630.
- Wang, L., Wen, L., Xu, C., Chen, J., Wang, X., Yang, L., Wang, W., Yang, X., Sui, X., Yao, L., Zhang, Q., 2015a. HONO and its potential source particulate nitrite at an urban site in North China during the cold season. *Sci. Total Environ.* 538, 93–101.
- Wang, S., Zhang, Q.V., Martin, R., Philip, S., Liu, F., Li, M., Jiang, X., He, K., 2015b. Satellite measurements oversee China's sulfur dioxide emission reductions from coal-fired power plants. *Environ. Res. Lett.* 10, 114015.
- Wang, T., Wang, P., Theys, N., Tong, D., Hendrick, F., Zhang, Q., Van Roozendaal, M., 2018. Spatial and temporal changes in SO₂ regimes over China in the recent decade and the driving mechanism. *Atmos. Chem. Phys.* 18, 18063–18078.
- Wang, Z., Wang, T., Guo, J., Gao, R., Xue, L., Zhang, J., Zhou, Y., Zhou, X., Zhang, Q., Wang, W., 2012. Formation of secondary organic carbon and cloud impact on carbonaceous aerosols at Mount Tai, North China. *Atmos. Environ.* 46, 516–527.
- Wu, L.Y., Tong, S.R., Wang, W.G., Ge, M.F., 2011. Effects of temperature on the heterogeneous oxidation of sulfur dioxide by ozone on calcium carbonate. *Atmos. Chem. Phys.* 11, 6593–6605.
- Xu, B., Shang, J., Zhu, T., Tang, X., 2011. Heterogeneous reaction of formaldehyde on the surface of γ-Al₂O₃ particles. *Atmos. Environ.* 45, 3569–3575.
- Yang, F., Tan, J., Zhao, Q., Du, Z., He, K., Ma, Y., Duan, F., Chen, G., 2011a. Characteristics of PM_{2.5} speciation in representative megacities and across China. *Atmos. Chem. Phys.* 11.
- Yang, F., Tan, J., Zhao, Q., Du, Z., He, K., Ma, Y., Duan, F., Chen, G., Zhao, Q., 2011b. Characteristics of PM_{2.5} speciation in representative megacities and across China. *Atmos. Chem. Phys.* 11, 5207–5219.
- Yao, L., Garmash, O., Bianchi, F., Zheng, J., Yan, C., Kontkanen, J., Junninen, H., Mazon, S.B., Ehn, M., Paasonen, P., Sipilä, M., Wang, M., Wang, X., Xiao, S., Chen, H., Lu, Y., Zhang, B., Wang, D., Fu, Q., Geng, F., Li, L., Wang, H., Qiao, L., Yang, X., Chen, J., Kerminen, V.-M., Petäjä, T., Worsnop, D.R., Kulmala, M., Wang, L., 2018. Atmospheric new particle formation from sulfuric acid and amines in a Chinese megacity. *Science* 361, 278.
- Yu, T., Zhao, D., Song, X., Zhu, T., 2018. NO₂-initiated multiphase oxidation of SO₂ by O₂ on CaCO₃ particles. *Atmos. Chem. Phys.* 18, 6679–6689.
- Zhang, J.K., Sun, Y., Liu, Z.R., Ji, D.S., Hu, B., Liu, Q., Wang, Y.S., 2014. Characterization of submicron aerosols during a month of serious pollution in Beijing, 2013. *Atmos. Chem. Phys.* 14, 2887–2903.
- Zhang, Q., Shen, Z., Cao, J., Zhang, R., Zhang, L., Huang, R.J., Zheng, C., Wang, L., Liu, S., Xu, H., Zheng, C., Liu, P., 2015. Variations in PM_{2.5}, TSP, BC, and trace gases (NO₂, SO₂, and O₃) between haze and non-haze episodes in winter over Xi'an, China. *Atmos. Environ.* 112, 64–71.
- Zhang, Y., Tong, S., Ge, M., Jing, B., Hou, S., Tan, F., Chen, Y., Guo, Y., Wu, L., 2018. The formation and growth of calcium sulfate crystals through oxidation of SO₂ by O₃ on size-resolved calcium carbonate. *RSC Adv.* 8, 16285–16293.
- Zhao, D., Song, X., Zhu, T., Zhang, Z., Liu, Y., Shang, J., 2018. Multiphase oxidation of SO₂ by NO₂ on CaCO₃ particles. *Atmos. Chem. Phys.* 18, 2481–2493.
- Zhao, D., Zhu, T., Chen, Q., Liu, Y., Zhang, Z., 2011. Raman micro-spectrometry as a technique for investigating heterogeneous reactions on individual atmospheric particles. *Sci. China Chem.* 54, 154–160.
- Zhao, P.S., Dong, F., He, D., Zhao, X.J., Zhang, X.L., Zhang, W.Z., Yao, Q., Liu, H.Y., 2013. Characteristics of concentrations and chemical compositions for PM_{2.5} in the region of Beijing, Tianjin, and Hebei, China. *Atmos. Chem. Phys.* 13, 4631–4644.